Study of Polymer Latex Coalescence by Dielectric Measurements in the Microwave Domain: Influence of Latex Characteristics

F. CANSELL, *Laboratoire d'Ingénierie des Matériaux et des Hautes Pressions, C.N.R.S., Université Paris-Nord, Avenue J.B. Clément, 93430 Villetaneuse, France,* F. HENRY, *Organisation Moléculaire et Macromoléculaire, C.N.R.S., 2, rue Henry Dunant, 94 320 Thiais, France,* and C. PICHOT, *Laboratoire des Matériaux Organiques, C.N.R.S., B.P. 24, 69390 Vernaison, France*

Synopsis

The coalescence process of polymer latex particles has been investigated by following simultaneously weight losses and dielectric constants variations during water evaporation in a latex deposited as a film in a resonant cavity at microwave frequency (5 GHz) and under controlled humidity and temperature. Different styrene (S) *n*-butyl acrylate (BuA) emulsion copolymer latexes were examined so as to differentiate the behaviors of film forming or non-film-forming latexes. In the latter ones, both flocculation and maximum packing points were clearly evidenced, whereas only the first point was shown in the former ones. The effect of other colloidal variables (particle size distribution, surface charge density, particle diameter, ionic strength) have also been studied. It is found that the influence of the last three parameters is reflective of the latex stability and can be well detected by dielectric measurement. Such a method appears to be quite reliable for studying the film-forming process of latexes having different colloidal characteristics.

INTRODUCTION

The mechanism of film formation from latexes has been thoroughly studied by several workers.[1-16] Three major steps have been characterized and well evidenced in the film-forming phenomenon: (1) the first one corresponds to water evaporation until the compact packing of polymer particles; (2) the second one corresponds to the deformation of polymer particles from a spherical shape to a more compact one (probably dodecahedral shape), so that all the particle surfaces are in contact—this leads to the film formation; (3) the last one corresponds to the gradual interdiffusion of macromolecular chains which makes the properties of the film to be improved (for example permeability, mechanical strength). However, few techniques, except the study of the weight losses variations,[17] allow us to follow dynamically the film-forming process of high water content latexes and discriminate these three steps. In a previous work,[18-21] we evidenced the various steps occurring during water evaporation of latex using a new methodology based on the small perturbation theory of microwave resonant cavities. This latter allows to follow quasi-specifically and precisely the water circulation was already applied in many phenomena where water–materials interactions play a predominant role.[22] Indeed, the "free" water molecule reaches a maximum of dipolar absorption in the microwave frequency domain

Journal of Applied Polymer Science, Vol. 41, 547–563 (1990)
 CCC 0021-8995/90/3-40547-17$04.00

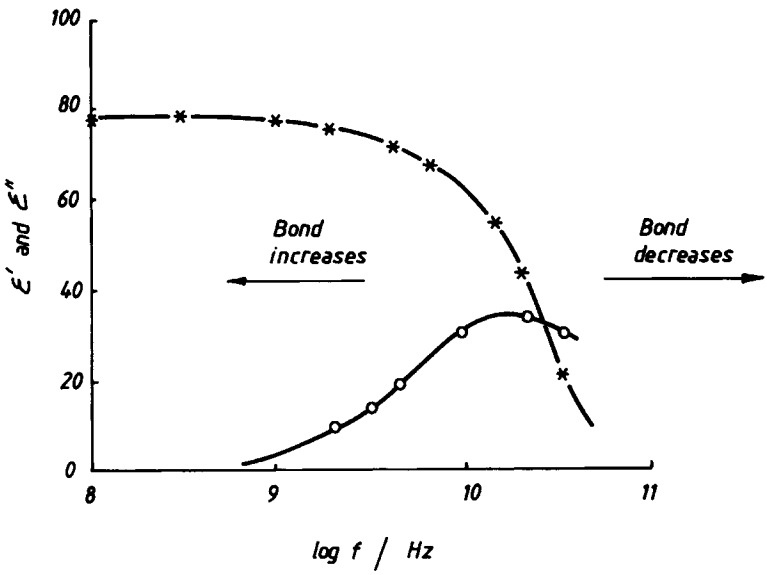

Fig. 1. Influence of the frequency on the dielectric properties of pure water at 25°C (24), ϵ' = relative permittivity (*), ϵ'' = dielectric losses = ϵ'' dipolar + ϵ'' conductive (0).

(Fig. 1). These cavities were conceived so as to measure simultaneously the variations (in real time) of dielectric constants (ϵ' and ϵ'') and the weight losses (with a microbalance) of macromolecular latexes during the film formation. The experiments were performed at 5 GHz at a constant temperature and under controlled atmosphere.

This article aims at giving more information on the film-forming process from latexes using this methodology. The influence of the latex characteristics has been systematically investigated including the glass transition temperature of the polymer, the particle size, the ionic strength of the aqueous medium, the presence of an emulsifier, and the surface charge density of the particles.

EXPERIMENTAL METHOD

Theory and Experimental Set-Up

When a dielectric specimen (nonmagnetic material) is inserted into a radio frequency resonant cavity, the configuration of the electric field (E) changes, and both the quality factor (Q) and the resonance frequency (F) are altered. Starting from Maxwell's equations, the perturbation formula can be derived giving[24]

$$\frac{(F - F_0)}{F_0} + j\left(\frac{1}{2Q} - \frac{1}{2Q_0}\right) = -\epsilon_0(\epsilon^* - 1)\frac{\iiint_v EE_0 dv}{4u} \qquad (1)$$

where:

ϵ^* is the relative complex permittivity;

$\epsilon_0 = 8{,}85\ 10^{-12}$ F/m;

E and E_0 are the perturbed and unperturbed electric fields in the region of the dielectric;

u relates to the total stored energy in the cavity;

v is the sample volume;

F, F_0 and Q, Q_0 are the perturbed and unperturbed frequencies and the corresponding Q-factors of the cavity respectively.

The relative complex permittivity (ϵ^*) is expressed by

$$\epsilon^* = \epsilon' - j\epsilon'' \qquad j^2 = -1 \tag{2}$$

where ϵ' and ϵ'' are the relative permitivity and the dielectric losses respectively. After integration and separation of the real and imaginary parts using Eq. (1) it becomes[24]

$$\frac{F - F_0}{F_0} = k_1(\epsilon' - 1)\frac{v}{V} \tag{3}$$

$$\frac{1}{Q} - \frac{1}{Q_0} = \frac{k_1}{2}\epsilon''\frac{v}{V} \tag{4}$$

where V is the cavity volume and K_1 is usually called "shape factor" or "depolarization factor" (corresponding to the ratio of the electric field in the material to the excitating electric field in the resonant cavity).

Therefore, the frequency shift is directly proportional to the material permittivity and the level of transmission (ζ) (quadratic detector cristal) is directly proportional to the Q-factor (ζ = constant. Q^2) then, to the dielectric losses.

For ionic materials, ϵ'' is given by:

$$\epsilon'' = \epsilon''_d + \frac{\sigma}{\omega\epsilon_0} \tag{5}$$

where σ is the ionic conductivity, ω the angular frequency of the electric field and ϵ''_d the dipolar dielectric losses.

The experimental set-up (Fig. 2) has already been described in a previous article[20] and the conditions of a typical experiment are as follows

frequency: 5 GHz
cavity TE 0,1,7 mode (Fig. 3)
field parallel to the support (glass)
sample deposited as a film
relative humidity: 38%
temperature: 28°C

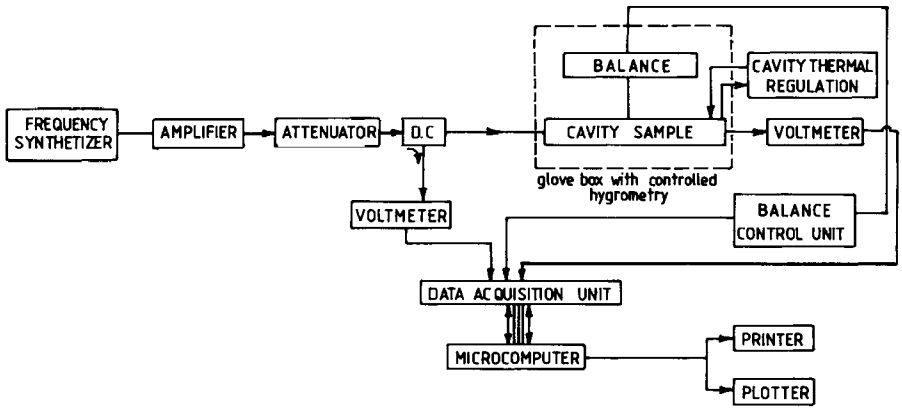

Fig. 2. Experimental set-up.

All the experiments were carried out using the same initial conditions so as to compare the results concerning the different latexes

weight of latex = 20 ± 1 mg
solid content of latex (wt %) = 30 ± 1%
surface of the film in the sample cell = 1 ± 0.1 cm^2

Preparation of Latexes

The monomers (styrene (S) and *n*-butyl acrylate (BuA) (from PROLABO)) were purified by distillation at 40 to 50°C under a N_2 atmosphere at a pressure of 5 mmHg. Azocarboxy (4,4′ azobis (4 cyanopentanoic acid) (kindly supplied

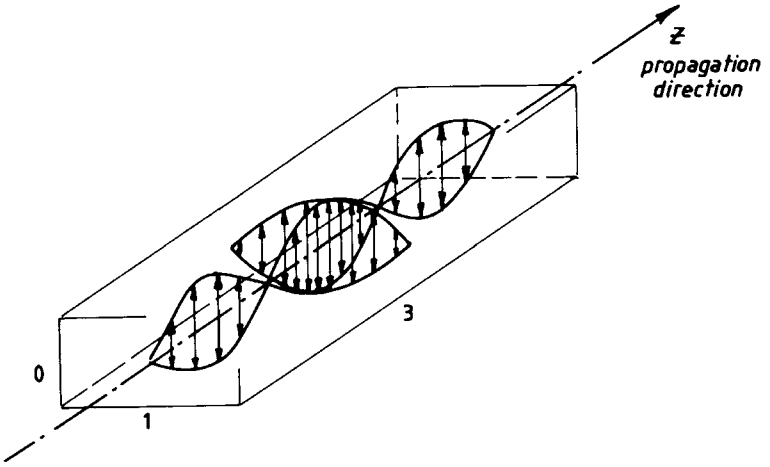

Fig. 3. Electric field distribution along the cavity for the TE 0,1,3 mode (TE = Transverse

TABLE I
Emulsion Polymerization Recipe for Latexes for Series A[a]

Ingredient	Amount, g
Water	200.0
Monomer mixture	80.0
Azocarboxy	0.164
$NaCO_3H$	0.196
SPM	0.560
SDS[b]	0.900

[a] Temperature: 64°C, Azocarboxy: 4,4′ azobis (4 cyanopentanoic), SPM: sulfopropyl methacrylate, SDS: sodium dodecylsulfate.
[b] Only for latex L13.

from SFOS)), sulfopropylmethacrylate (SPM) (kindly supplied from Rashig) and sodium hydrogenocarbonate (from Prolabo) were used as received. The latexes were prepared by batch emulsifier-free polymerization either in the presence of the sulfopropylmethacrylate (A, Table I) or according to the procedure described by OTTEWILL and co-workers[32] (Table II).

Characterization of Latexes

The copolymer composition was determined by ^{1}H-NMR using a Brucker CW 80 (at a temperature of 75°C, $CDCl_3$, solvent and HMDS reference) (Table III). The glass temperature transition of copolymers was determined by differential scanning calorimetry using a Perkin–Elmer DSC 4 instrument. The particle size was measured by QELS using a Nanosizer (from COULTRONICS) or a Malvern equipment.

After latex cleaning into mixed-bed resins (Dowex 50, Dowex 1) the surface end-group concentration was determined by conductimetric titration using a Tacussel equipment, from which the surface charge was deduced.

RESULTS AND DISCUSSION

The variations of the weight solid contents of the latex, the frequency (F) and the inverse of the Q-factor ($1/Q$) were recorded as a function of time. Using the measurements in real time of the sample weight, the variations of

TABLE II
Emulsion Polymerization Recipe for Latexes for Series B[a]

Ingredient	Amount, g
Water	800
Styrene	2 to 80 (variable)
NaCl	0.505
$K_2S_2O_8$	0.596

[a] Temperature: 77°C.

TABLE III
Characteristics of S/BuA Copolymer or PS Homopolymer Latexes

Latex code	Type of synthesis	Styrene composition in mole % (from ^{1}H-NMR)	Particle diameter in nm (from Nanosizer)	Glass transition temperature[a] (°C)
L1	A	100	170	104
L2	A	80	210	53
L3	A	66	197	31
L4	A	40	243	−10
L5	A	19	240	−35
L6	A	0	248	−52
L7	B	100	165	104
L8	B	100	204	104
L9	B	100	285	104
L10	B	100	380	104
L11	B	100	770	104
L12	B	100	990	104
L13[b]	A	21	150	−34
L14	A	100	217	104

[a] Determined by differential scanning calorimetry.
[b] Prepared in the presence of SDS.

F, $(1/Q)$, and (dW/dt) (rate of weight losses) were expressed as a function of the weight percentage of latex particles (wt %). Such a representation permits a good normalization of the different results and it was used throughout this article.

Influence of Glass Temperature Transition (T_g)

The variations of F, $(1/Q)$, and (dW/dt) are illustrated as a function of the wt % for two types of latexes (Table IV); a non-film-forming one (Fig. 4)

TABLE IV
Effect of Glass Transition Temperature (T_g) of Polymers on the Dielectric and Weight Variations

Latex code	Styrene content in mole %	T_g (°C)	Wt % at point A (%)	Wt % at point B (%)	Slope value $(d(1/Q)/dt)$[a] (in arbitrary units (AU)) Step I AU·mn^{-1}	Step II AU·mn^{-1}	Step III AU·mn^{-1}
L1	100	104	50	65	−2.8	−1.9	−4.3
L2	80	53	48	64	−2.7	−2.0	−4.3
L3	66	31	52	64	−2.8	−1.7	−4.2
L4	40	−10	61		−2.7		−2.3
L5	19	−35	60		−2.8		−2.2
L6	0	−52	61		−2.8		−2.4

[a] Precision on the slope values = 0.1 (AU); Q = Q-factor of cavity; wt % = weight percentage on polymer particle.

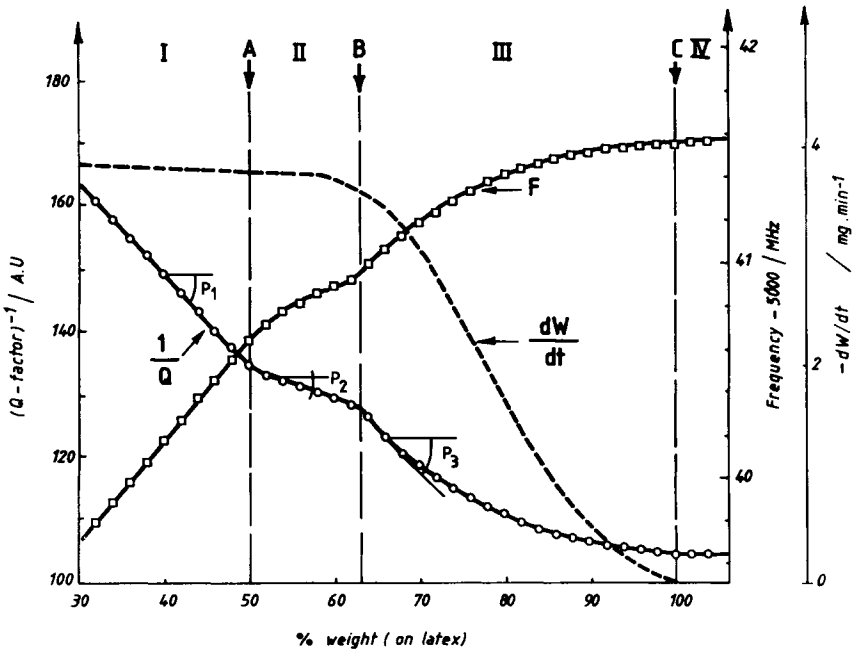

Fig. 4. Dielectric (F and $1/Q$) variations and weight losses rate as a function of % weight (on latex) for latex sample L1.

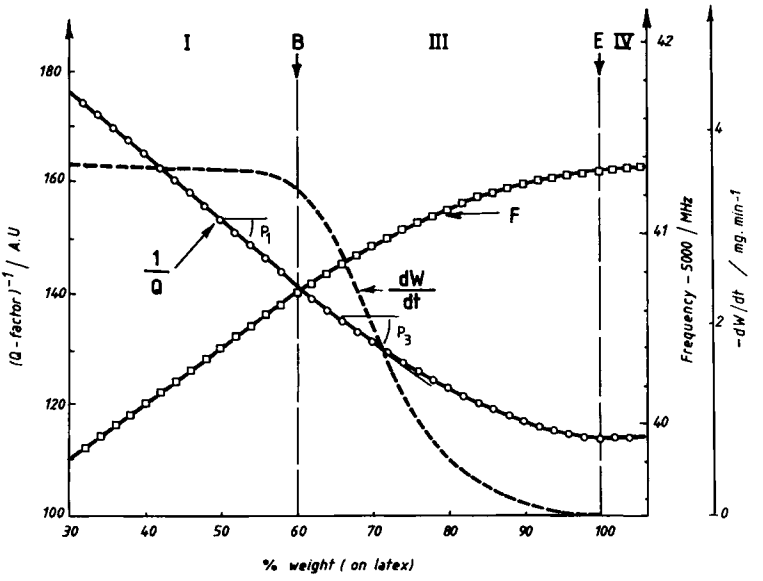

Fig. 5. Dielectric (F and $1/Q$) variations and weight losses rate as a function of % weight (on latex) for latex sample L4.

and a film-forming one (Fig. 5). In previous works,[18–21] the dielectric parameters variations were shown to exhibit distinct steps which are briefly recalled hereafter.

Non-film Forming Latex

The dielectric parameters variations for latex L1 are presented in Figure 4. For samples L2, L3, L7 to L12, and L14, which are also non-film-forming latexes at ambient temperature, the curves were found to exhibit the same behavior.

During step I, the polymer concentration increases; since the polymer dielectric constants are smaller than the water ones (ϵ' water = 73.2, ϵ'' water = 17.2, ϵ' polymer = 2.5, ϵ'' polymer = 10^{-2}; at 5 GHz and 20°C),[23] therefore both the whole relative permittivity and the dielectric losses decrease. Furthermore, this decrease was found to be dependent on external conditions such as temperature and relative humidity.[21]

At point A, the emulsion starts to flocculate and reaches the maximum packing at the end of step II. It is worthy to note a modification of the slope in the F and $1/Q$ variations. The increase of $1/Q$ can be interpreted by double layers repulsion of particles coming into contact, leading to an overall increase of the ionic conductivity (σ) (see Eq. (5)).

Between points A and B, the lowering of the frequency increase can be interpreted by:

1. a desorder to order transition (leading, for example, to a face centered cubic or a hexagonal close packed structure or to a mixture of cubic and hexagonal close packed structures). But the increase of the compaction creates a transient porosity by the rolling process (dilatancy phenomenon[25,26]).
2. the exclusion of water, less interacting with the surface of the particles, which would have its maximum of dipolar relaxation shifted to the high frequencies : the direct consequence was an increase of ϵ' and a reduction of the F decrease (Fig. 1).

After point B the dielectric parameters show strong variations and the rate of weight losses rapidly drops (Fig. 4). At point B, the space filling of packing should be maximum (Table IV). Indeed, it almost corresponds to 64 wt % which corresponds to the compaction percentage mentioned in the literature for a dense random packing of monodisperse particle diameters (50% cubic and 50% compact hexagonal).[27,28]

The dehydration process which involves the evaporation of bulk water (partially affected by the external conditions) is now due to the evaporation of capillary water (partially affected by the internal characteristics of the compact materials). Water, which was the continuous phase, becomes the dispersed one and diffuses within a packing of spheres. Beyond point C, the weight losses and the dielectric parameters do not change anymore and the film stops its macroscopic evolution.

Film Forming Latex

The dielectric parameters variations for latex L4 are reported in Figure 5. For the other film-forming latexes (samples L5, L6, L13) the curves also displayed the same steps than in Figure 5.

Step I was similar to the one described for non-film-forming latexes. On the contrary, the plateau corresponding to step II in non-film-forming latexes was no more observed (Fig. 5). The particles in a film-forming latex can be distorted so that:

on the one hand, this distortion would induce a progressive decrease of the water polymer interface without leading to an increase of the ionic conductivity (σ) of the mixture (the reverse was true for non-film-forming latexes);

on the other hand, the sample volume decreased until point C;

moreover, this distortion would prevent the water ejection between particles because water can hardly circulate.

At point B, a steep drop of the rate of weight losses occurs, therefore, point B would be characteristic of the beginning of the latex coalescence. Then, the volume between particles progressively decreases so that water evaporation process is more and more difficult. The rate of weight losses, rapidly falling, was in accordance with this interpretation. Furthermore, in step III, the absolute value of the slope (Table IV), given by $d(1/Q)/dt$, was very much inferior for film-forming latexes than for non-film-forming ones showing that water hardly evaporates when the polymer matrix distorts.

After point C, although the latex film morphology continues to change (further gradual coalescence process),[10,11] no variation of F and $(1/Q)$ is detected. As a matter of fact, the film is almost free of water (wt % = 99.7).

Influence of Particle Size Distribution

The wt % variations at point B were studied for different mixtures containing two particle size distributions (as reported in Table V). Using the mathematical model for a binary mixture of two spherical distributions,[27] several latexes were prepared. For each of them, the wt % values at point B were compared to the theoretical data corresponding at the maximum compaction. The experimental wt % values at point B follow the variations of the theoretical data but always remained inferior to them. This could be interpreted by the fact that the math-

TABLE V
Effect of the Binary Mixture Composition on the Wt % (on Polymer Particle) Values at Point B

Latex code	ϕ_l[a] (nm)	ϕ_s (nm)	γ_s[b]	Wt % at point B (%)	Theoretical compacity for random packing
L7	165			64	64
L9	285			64	64
L10	380			66	64
L11 + L8	770	204	0.265	69	71.8
L12 + L8	990	204	0.265	72	75.5
L12 + L7	990	165	0.265	74	79.2

[a] ϕ_l = diameter of large particles. ϕ_s = diameter of small particles.
[b] γ_s = volume fraction of small particles; $\gamma_l + \gamma_s = 1$.

ematical model of compaction does not take into account the real physic state of the latex particle surface on which functional groups are chemically anchored and in some cases the presence of hydrosoluble polymers physically adsorbed. That prevents the small particles to fill quite well the void between the large particles and leads to an actual compaction point (point B) appearing to a smaller solid content. In conclusion, the wt % values at point B correspond to the maximum point of compaction of this latter and should critically depend on the colloidal characteristics of the latex as it will be evidenced below.

Influence of the Particle Diameter and of the Medium Ionic Strength

The variations of F and $(1/Q)$ were studied first as a function of the particle size and second as a function of the medium ionic strength. Table VI summarizes the results concerning the influence of the particle diameter for monodisperse polystyrene latexes with similar surface charge densities. Only the value of the slope $(d(1/Q)/dt)$ in step II is found to vary with the particle diameter. The smaller the particle diameter, the lower the slope value appears.

In order to give an interpretation of the results, the theory of latex stability is briefly recalled. During the particle flocculation, the aggregation rate is given by[30]

$$\frac{dN}{dt} = \frac{k_0 N_0}{W} \tag{6}$$

with:

N = number of particles at time t
N_0 = initial number of particles per unit volume ($t = 0$)
k_0 = diffusion controlled rate constant for rapid coagulation
W = stability ratio (Fuch's ratio) given by:

$$W = 2a \int_0^\infty \frac{\exp(V_T/kT)\,dh}{(h + 2a)^2} \tag{7}$$

TABLE VI
Effect of Particle Diameter on the Dielectric Constants Variations

Latex code	Particle diameter (nm)	Surface charge density $\mu \cdot cm^{-2}$	Slope value $d(1/Q)/dt$ (in arbitrary units (AU))[a] Step I $AU \cdot mn^{-1}$	Step II $AU \cdot mn^{-1}$	Step III $AU \cdot mn^{-1}$
L7	165		−2.8	−1.9	−4.3
L8	204	5.7	−2.8	−1.9	−4.1
L9	285		−2.7	−2.1	−4.1
L10	380	5.4	−2.8	−2.2	−4.2
L11	770	5.1	−2.7	−2.3	−4.3

[a] Precision = 0.1 (AU).

where V_T is the height of the energy barrier, h is the distance between two particles of radius a.

From these formula, it can be deduced that an increase of the particle radius leads to a decrease of W, then to an increase of the aggregation rate. Consequently, the value of the slope obtained in step II is a function of the latex stability and therefore to the magnitude of the energy barrier (V_T) (corresponding to the energy for particles coming into contact[30]).

The effect of the ionic strength was investigated on two non-film-forming latexes which have been preliminary cleaned by ion exchange on a mixed-bed (Dowex 50, Dowex 1) resins (conductivity $\sigma = 0.2\ \mu S$),[31] and the second one containing 0.2 mol l^{-1} of $NaCO_3$ H (conductivity $\sigma = 0.5$ mS). The general shapes of the curves were similar to those previously obtained for non-film-forming latexes (Fig. 4), however, the values of $(d(1/Q)/dt)$ in step II were found to decrease with an increase of the medium ionic strength (Table VII). It has long been recognized that the stability of a latex decreases when increasing the ionic strength of the aqueous medium.[30] Consequently, it appears that the slope values could directly provide information about the latex stability: the lower the slope value, the less stable the latex does appear. According to the DLVO theory of the colloidal stability,[30] for two interacting particles having the colloidal characteristics of latex L3, the potencial energy (V_T) versus the interparticle distance h is presented on Figure 7 for different ionic strength values. Smaller ionic strengths result in more stable latexes. Although this approach of the latex stability is far to be representative of the reality (since in concentrated dispersions multiinteracting particles should be taken into account), qualitatively there is a good agreement between these predictions and the results previously mentioned. Hence, the value of $d(1/Q)/dt$ in step II is indeed reflective of the latex stability which is dependent on particle size or ionic strength variations.

Influence of the Surface Charge Density

The behavior of three film-forming latexes exhibiting various surface charge densities has been investigated so as to examine the influence of this important parameter. Sample L4 is characterized by a low surface charge density (Table VIII) whereas sample L4* (obtained after postpolymerization of the sulfonate

TABLE VII
Effect of Medium Ionic Strength on the Dielectric Constants Variations

Latex code	Particle diameter (nm)	Surface charge density (μ cm^{-2})	Slope value $d(1/Q)/dt$ (in arbitrary units (AU)[a] in step II: Deionized latex (AU mn^{-1})	Slope value $d(1/Q)/dt$ (in arbitrary units (AU)[a] in step II: Deionized latex + 0, 2 mol L^{-1} of $NaCO_3H$ (AU mn^{-1})
L3	197	7, 9	−1.7	−2.2
L7	165		−1.9	−2.3
L8	204	5, 7	−1.9	−2.2

[a] Precision = 0.1 (AU).

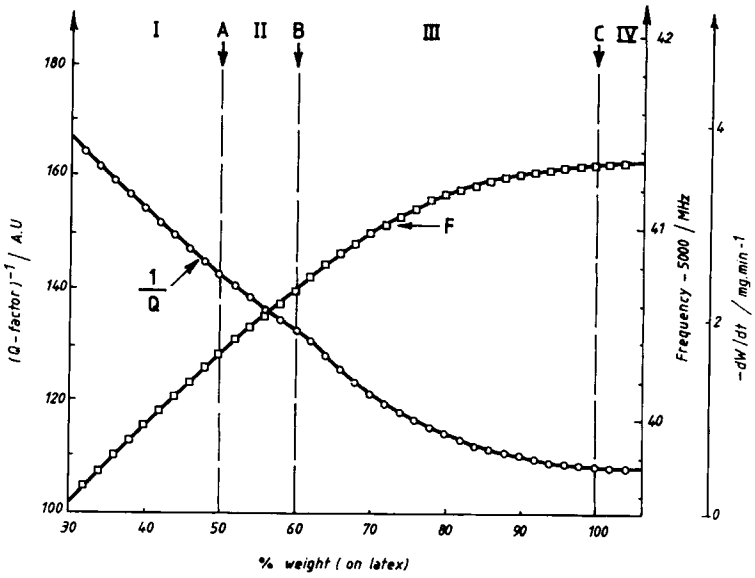

Fig. 6. Dielectric (F and $1/Q$) variations as a function of % weight (on latex) for latex sample L13 (synthetized with the SDS as emulsifier).

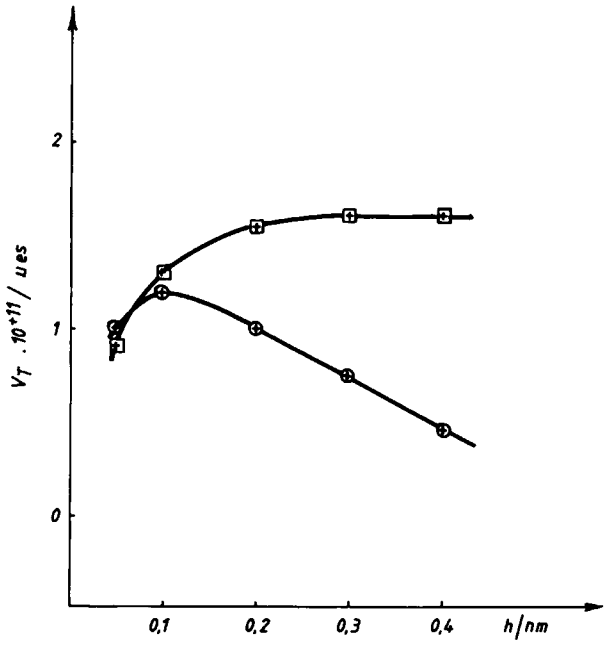

Fig. 7. V_T against interparticle distance for spherical particles at various ionic strengths (I) with Hamaker constant A = 5.10^{-14} erg at 25°C for latex sample L3 (ϕ = 197 nm, σ_s = 7.9 μc. cm^{-2}); I = 10^{-4} mol L^{-1} (□) and I = 0.2 mol L^{-1} (○).

TABLE VIII
Surface Properties of Three S/BuA Copolymer Latexes

Latex code	Particle diameter (nm)	T_g (°C)	Surface end group (SO_4^-) concentration (μ cm^{-2})
L13[a]	150	−36	13.5
L4	243	−10	4.6
L4*[b]	243	−10	25.9

[a] Prepared in the presence of SDS.
[b] Latex (L4) has been poststabilized with the functional comonomer (SPM).

comonomer SPM into latex L4) and sample L13 (prepared in the presence of SDS) display higher surface charge densities (Table VIII). For the initial latex (Sample L4), the variations of the dielectric parameters have been already given in Figure 5. For the two other latexes (Samples L13 and L4*) the curves were similar whatever the method used for increasing the surface charge density. Figure 6 displays the variations of the dielectric parameters for the latex (L13) prepared in the presence of SDS. This curve can be compared to the one obtained for a non-film-forming latex (Fig. 4) where four steps were already evidenced. However, the variations of $(1/Q)$ in step II and the beginning of step III were less visible. A possible interpretation is that, when the particles begin to come into contact, the stabilizing functions would behave like a rigid layer, opposed to the distortion of latex particles. But, this opposite effect is not permanent because the film-forming process continues to occur, with a possible rearrangement of the stabilizing end groups within the film.

As already observed in a previous work[29] for particles having the same diameter, the value of wt % at point B has been shown to increase with the quantity of surface end groups (Table IX). This has been interpreted by a rearrangement of the latex particles, during water evaporation: the stronger the electrostatic repulsion, the nearer the compacity values (point B), evaluated from the theoritical value of the maximum point of compaction, will be. The latter increases with the surface charge density. When the surface charge density increases the dense random packing is replaced by a compact hexagonal packing where the theoritical compacity is 74%. Using the same DLVO simulation, the value of the potencial energy (V_T) versus the interparticle distance was cal-

TABLE IX
Effect of the Surface Charge Density on the Wt % (on Polymer Particle) Values at Point B

Latex code	Particle diameter (nm)	Surface charge density (μ cm^{-2})	Wt % at point B (%)
L8	204	5.7	62
L14	217	30	71
L4	243	4.6	61
L4*	243	25.9	65

culated for the latexes L4, L13, and L4* having various surface charge density (Fig. 8). It is noteworthy that latex sample L4* is much more stable than latex sample L4 so that the electrostatic repulsion forces are stronger in L4* sample than in L4 one. This is in agreement with the results previously mentioned.

It is worth understanding the physical meaning of the slope value, $d(1/Q)/dt$, especially in the steps I and II. $d(1/Q)/dt$ is given by the following expression:

$$\left(\frac{1}{Q}\right) = k_2 \epsilon'' v \tag{8}$$

where k_2 is a constant deduced from Eq. (4).

Concerning the dielectric losses constitution (ϵ'') it can be expressed by a mixing law:

$$\epsilon'' v = \epsilon''_w v_w + \epsilon''_p v_p \tag{9}$$

where v_w and v_p are the volume of aqueous and polymer phase respectively, with

$$v = v_p + v_w$$

Applying Eq. (5) for the polymeric phase:

$$\epsilon''_p = \epsilon''_{dp} + \frac{\sigma_p}{\omega \epsilon_0}$$

ϵ''_p can be expressed by the following expression:

$$\epsilon''_p = \epsilon''_{dp} + \frac{k_3 N_s}{v_w} \tag{10}$$

where k_3 is a constant including $1/\omega\epsilon_0$ and N_s is the total surface charge number (for all particles) in the medium.

Combining Eqs. (8), (9) and (10), it follows

$$\left(\frac{1}{Q}\right) = k_2 \left(\epsilon''_w v_w + \epsilon''_{dp} v_p + k_3 N_s \frac{v_p}{v_w} \right) \tag{11}$$

Knowing that only v_w is varying after derivation of Eq. (11) it comes

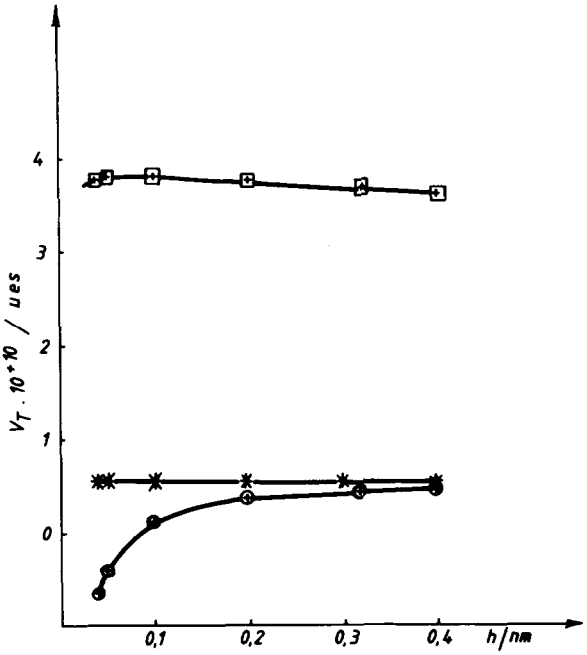

Fig. 8. V_T against interparticle distance for spherical particles at various surface charge densities σ_s) with constant ionic strength (10^{-3} M), Hamaker constant A = 5.10^{-14} erg at 25°C; (□): latex sample L4* (ϕ = 243 nm, σ_s = 25.9 μc.cm^{-2}); (○): latex sample L4 (ϕ = 243 nm, σ_s = 4.6 μc.cm^{-2}); (*): latex sample L13 (ϕ = 150 nm, σ_s = 13.5 μc.cm^{-2}).

$$\frac{d\left(\frac{1}{Q}\right)}{dt} = k_2\left(\epsilon''_w \frac{dv_w}{dt} + k_3 N_s v_p \frac{d\left(\frac{1}{v_w}\right)}{dt}\right) \tag{12}$$

$$\frac{d\left(\frac{1}{Q}\right)}{dt} = k_2 \frac{dv_w}{dt}\left(\epsilon''_w - k_3 \frac{N_s v_p}{v_w^2}\right) \tag{13}$$

During the water evaporation we observe simultaneously

1. v_w decreases and $\frac{dv_w}{dt} < 0$
2. $\frac{v_p}{v_w^2}$ increases, because we consider v_p and N_s both constant.

So, greater the surface charge number (N_s), lower the difference $\left(\epsilon''_w - \frac{k_2 N_s v_p}{v_w^2}\right)$ is which becomes negative; then the derivative $\frac{d(1/Q)}{dt}$ becomes positive.

Applying Eq. (13), it is possible to compare the two latex samples E_1 and E_2, where E_1 is characterized by a lower surface charge number than E_2 (N_{s1}

$< N_{s2}$) (all other characteristics being the same). Latex E_1 being less stable than latex E_2, then it will flocculate more rapidly than E_2. Knowing that $\frac{dv_w}{dt}$ is negative, it comes:

$$\frac{d\left(\frac{1}{Q}\right)}{dt} E_2 > \frac{d\left(\frac{1}{Q}\right)}{dt} E_1$$

This is in agreement with the results previously reported concerning the variation of $(d(1/Q)/dt)$ in step II which shows the predominant effect of the surface charge density.

CONCLUSION

This methodology, based on simultaneous measurement of dielectric constants at microwave frequency and weight losses variations of latex, seems to be well adapted for studying the polymer latex coalescence. The main results can be summarized as follows: (1) it permits to distinguish the behaviour between film-forming latexes and non-film-forming ones; (2) both the flocculation and the maximum points of compaction for non-film-forming latexes can be evidenced; (3) the influence of both the particle size and of the medium ionic strength on the dielectric parameters variations can be also taken into account; (4) the analysis of latex exhibiting various surface charge densities would suggest that the surface end groups behave like a rigid layer opposed to the distortion of latex particles. The study of the dielectric parameters variations as a function of the various latex characteristics clearly shows the predominant effect of the energy barrier to cause the coalescence of the latex particles which has to be overpassed.

References

1. R. E. Dillon, L. A. Matheson, and E. B. Bradford, *J. Colloid Sci.*, **6**, 108 (1951).
2. G. R. Brown, *J. Polymer Sci.*, **22**, 423 (1956).
3. E. B. Bradford and J. W. Vanderhoff, *J. Macromol. Chem.*, **1**, 335 (1966).
4. J. W. Vanderhoff, H. L. Tarkowski, M. C. Jenkins, and E. B. Bradford, *J. Macromol. Chem.*, **1**, 361 (1966).
5. G. Masson, *Br. Polym. J.*, **5**, 101 (1973).
6. S. S. Voyutskii, *J. Polymer. Sci.*, **32**, 528 (1958).
7. K. L. Johnson, K. Kendall, and A. D. Roberts, *Proc. Roy. Soc., London*, **A 324**, 301 (1971).
8. K. Kendall and J. C. Padget, *Int. J. Adh.*, **2**, 149 (1982).
9. J. Lamprecht, *Colloid Polym. J.*, **258**, 960 (1980).
10. W. A. Cote, A. C. Day, G. W. Wilkes, and R. Marchessault, *J. Colloid Interface Sci.*, **27**, 32 (1968).
11. M. Chainey, M. C. Wilkinson, and J. Hearn, *J. Polymer. Sci., Poly. Chem. Ed.*, **23**, 2947 (1985).
12. D. P. Sheetz, *J. Appl. Polym. Sci.*, **9**, 3759 (1963).
13. M. S. El-Aasser and A. A. Robertson, *J. Colloid Interface Sci.*, **36**, 86 (1971).
14. A. Homola and A. A. Robertson, *J. Colloid Interface Sci.*, **54**, 286 (1976).
15. J. T. Lin, M. S. El-Aasser, C. A. Silebi, and J. W. Vanderhoff, *J. Colloid Interface Sci.*, **110**, 305 (1986).

16. K. Hahn, G. Ley, H. Schuller, and R. Oberthur, *Colloid Polym. J.*, **264,** 1096 (1986).
17. J. W. Vanderhoff, *Polym. News,* **3**(4), 194.
18. F. Henry, J. L. Guillaume, and F. Cansell, *FATIPEC proceeding,* 376 (1985).
19. F. Cansell and F. Henry, *FATIPEC proceeding,* 234 (1987).
20. F. Cansell and F. Henry, *Makromol. Chem., Macromol. Symp.,* **23,** 401 (1989).
21. F. Henry, F. Cansell, J. L. Guillaume, and C. Pichot, *Colloid Polym. Sci.,* **267,** 167 (1989).
22. F. Henry, Thesis, University of Paris VI (1982).
23. R. Von Hippel, *Dielectric Materials and Applications,* Chaphan and Hall, London, 1954.
24. A. C. Metaxas and R. J. Meredith, *Industrial Microwave Heating,* Peter Peregrinus Publisher, London, 1983, p. 26.
25. J. P. Bombled, *Rev. Materiaux de Construction,* 688 (1974).
26. P. C. Hiemenz, *Principles of Colloid and Surface Chemistry,* Marcel Dekker, New York, 1986, p. 225.
27. D. I. Lee, *J. of Paint Technology,* **42,** 579 (1970).
28. A. I. Ranka, Thesis, Chemical Engineering, Lehigh University, 1984.
29. F. Henry, F. Cansell, P. Bailleuil, A. Brandt, and P. Noe, *Symposium on Applications Energétiques des Mícroondes,* Paris 1987, p. 139.
30. R. Buscall and R. H. Ottewill, *Polymer Colloid,* Buscall, Corner, and Stageman, Eds., Elsevier, New York, 1985.
31. W. C. Wu, Thesis, Lehigh University, 1977.
32. J. W. Goodwin, J. Hearn, C. C. Ho, and R. H. Ottewill, *Br. Polym. J.*, **5,** 347 (1973).

Received February 22, 1989
Accepted August 23, 1989